Comparison of nucleon form factors from lattice QCD against the light front cloudy bag model and extrapolation to the physical mass regime

Hrayr H. Matevosyan
Louisiana State University, Department of Physics and Astronomy, 202 Nicholson Hall, Tower Dr., Baton Rouge, Louisiana 70803, USA and Thomas Jefferson National Accelerator Facility, 12000 Jefferson Ave., Newport News, Virginia 23606, USA

Gerald A. Miller
University of Washington, Department of Physics, Box 351560, Seattle, Washington 98195-1560, USA

Anthony W. Thomas
Thomas Jefferson National Accelerator Facility, 12000 Jefferson Ave., Newport News, Virginia 23606, USA
(Received 20 January 2005; published 23 May 2005)

We explore the possibility of extrapolating state of the art lattice QCD calculations of nucleon form factors to the physical regime. We find that the lattice results can be reproduced using the light front cloudy bag model by letting its parameters be analytic functions of the quark mass. We then use the model to extend the lattice calculations to large values of Q^2 of interest to current and planned experiments. These functions are also used to define extrapolations to the physical value of the pion mass, thereby allowing us to study how the predicted zero in $G_E(Q^2)/G_M(Q^2)$ varies as a function of quark mass.

DOI: 10.1103/PhysRevC.71.055204 PACS number(s): 13.40.Gp, 11.15.Ha, 12.38.Gc

I. INTRODUCTION

The electromagnetic form factors of the nucleon are an invaluable source of information on its structure [1]. For example, observing their fall as Q^2 increases from zero revealed the finite extent of the nucleon, and measuring the Sachs electric form factor of the neutron, G_E^n [2,3], that it has a positive core surrounded by a long-range, negative tail [4–6]. In the last few years particular interest has focused on the ratio of the electric and magnetic form factors of the proton, G_E/G_M, where recoil polarization data [7,8] have revealed a dramatic decrease with Q^2—in contrast with earlier work based on the Rosenbluth separation. These data have allowed one of us to deduce a fascinating spin dependence of the shape of the nucleon [9].

While the behavior of G_E/G_M with Q^2 was anticipated in some models (e.g., see Refs. [10,11]), there is no consensus as to which explanation best represents how QCD works. Direct guidance from QCD itself would be most valuable and for that purpose lattice QCD represents the one and only technique by which one can obtain nonperturbative solutions to QCD.

The QCDSF Collaboration recently presented lattice QCD simulations for the form factors of the nucleon over a wide range of values of momentum transfer [12]. While these were based on the quenched approximation, with an unsophisticated action, several lattice spacings were chosen with the smallest being around 0.05 fm ($\beta = 6.4$) and at present these are the state of the art. The quark masses used in the simulations correspond to pion masses in the range (0.6–1.2) GeV. Therefore one needs to parametrize the form factors as a function of pion mass and extrapolate to the physical value before comparing these lattice results with the experimental data.

At $Q^2 = 0$ there have been a number of studies of the chiral extrapolation of baryon magnetic moments [13–16]. However, there is no model independent way to respect the constraints of chiral symmetry over the range of Q^2 and m_π required by the QCDSF data. Instead, at finite Q^2, one has been led to study various phenomenological parametrizations [17], which have at least ensured the correct leading order nonanalytic structure as $m_\pi \to 0$. Our purpose here is threefold. First, we wish to use the lattice data to investigate whether a particular quark model is capable of describing the properties of the nucleon in this additional dimension of varying m_π—an important test which any respectable quark model should satisfy.[1] Second, having confirmed that the model is consistent with the lattice data over the range of m_π noted earlier, we use the model to extrapolate to large values of Q^2 (for lattice values of m_π). Third, we also use the model to extrapolate to the physical pion mass.

The model which we consider here is the light front cloudy bag model (LFCBM) [19], which was developed as a means of preserving the successes of the original cloudy bag model [6], while ensuring covariance in order to deal unambiguously with modern high energy experiments. The light front constituent quark model, upon which it is built [10], predicted the rapid decrease of G_E/G_M with Q^2 and, as the pion cloud is expected to be relatively unimportant at large Q^2, this success carries over to the LFCBM [19]. Furthermore the LFCBM corresponds to a Lagrangian built upon chiral symmetry, so it can be extended to the limit of low quark mass as well as low and high Q^2.

The outline of the paper follows. In Sec. II we briefly review the LFCBM. In Sec. III we present the lattice QCD data,

[1] Just as the study of QCD as a function of N_c has proven extremely valuable, so the study of hadron properties as a function of quark mass, using the results of lattice QCD calculations, undoubtedly offers significant insight into QCD, as well as new ways to model it [18].

explain the fitting procedure, and present the results. Section IV contains some concluding remarks.

II. REVIEW OF THE LFCBM

The light front cloudy bag model (LFCBM) respects chiral symmetry and Lorentz invariance and reproduces the four nucleon electromagnetic form factors. Therefore it is reasonable to try to use it to extrapolate the form factors computed using lattice QCD to the physical pion mass. We begin by briefly introducing the key features of the LFCBM.

The LFCBM is a *relativistic* constituent quark model incorporating the effect of *pion-loops*, key features motivated by chiral symmetry. The light-front dynamics is employed to maintain the Poincaré invariance, and one pion-loop corrections are added to incorporate significant pion cloud effects (particularly in the neutron electric form factor and magnetic moments) as well as the leading nonanalytic behavior imposed by chiral symmetry. In light-front dynamics the fields are quantized at a fixed "time" $= \tau = x^0 + x^3 \equiv x^+$. The light front time or τ-development operator is then $P^0 - P^3 \equiv P^-$. The canonical spatial variable is $x^- = x^0 - x^3$, with a canonical momentum $P^+ = P^0 + P^3$. The other coordinates are $\mathbf{x}_\perp$ and $\mathbf{P}_\perp$. The relation between the energy and momentum of a free particle is given by $p^- = (p_\perp^2 + m^2)/p^+$, with the quadratic form allowing the separation of center of mass and relative coordinates. The resulting wave functions are frame independent. The light front technique is particularly relevant for calculating form factors because one uses boosts that are independent of interactions.

Our goal is to calculate the Dirac F_1 and Pauli F_2 form factors given by

$$\langle N, \lambda' p' | J^\mu | N, \lambda p \rangle = \overline{u}_{\lambda'}(p') \left[F_1(Q^2)\gamma^\mu + \frac{F_2(Q^2)}{2M_N} i\sigma^{\mu\nu}(p'-p)_\nu \right] u_\lambda(p). \tag{1}$$

The momentum transfer is $q^\mu = (\ p' - p)^\mu$, $Q^2 = -q^2$ and J^μ is taken to be the electromagnetic current operator for a free quark. For $Q^2 = 0$ the form factors F_1 and F_2 are, respectively, equal to the charge and the anomalous magnetic moment κ in units of e and $e/(2M_N)$, and the magnetic moment is $\mu = F_1(0) + F_2(0) = 1 + \kappa$. The evaluation of the form factors is simplified by using the so-called Drell-Yan reference frame in which $q^+ = 0$, so that $Q^2 = q_\perp^2 = q_1^2$. If light-front spinors for the nucleons are used, the form factors can be expressed in terms of matrix elements of the plus component of the current [21]:

$$F_1(Q^2) = \langle N, \uparrow | J^+ | N, \uparrow \rangle$$

and

$$Q F_2(Q^2) = (-2M_N)\langle N, \uparrow | J^+ | N, \downarrow \rangle. \tag{2}$$

The form factors are calculated using the "good" component of the current, J^+, to suppress the effects of quark-pair terms. Finally, we note that in our fits we will use the Sachs form factors, which are defined as

$$G_E = F_1 - \frac{Q^2}{4M_N^2} F_2, \qquad G_M = F_1 + F_2. \tag{3}$$

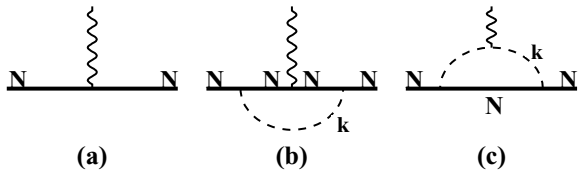

FIG. 1. Diagrams.

The next step is to construct the bare (pionless) nucleon wave function Ψ, which is a symmetric function of the quark momenta, independent of reference frame, and an eigenstate of the canonical spin operator. The commonly used ansatz is

$$\Psi(p_i) = \Phi\left(M_0^2\right) u(p_1)u(p_2)u(p_3)\psi(p_1, p_2, p_3), \qquad p_i = \mathbf{p}_i s_i, \tau_i, \tag{4}$$

where ψ is a spin-isospin color amplitude factor, the p_i are expressed in terms of relative coordinates, the $u(p_i)$ are Dirac spinors and Φ is a momentum distribution wave function. The specific form of ψ is given in Eq. (12) of Ref. [20] and earlier in Ref. [11]. This is a relativistic version of the familiar SU(6) wave function, with no configuration mixing included. The notation is that $\mathbf{p}_i = (p_i^+, \mathbf{p}_{i\perp})$. The total momentum is $\mathbf{P} = \mathbf{p}_1 + \mathbf{p}_2 + \mathbf{p}_3$, the relative coordinates are $\xi = p_1^+/(p_1^+ + p_2^+)$, $\eta = (p_1^+ + p_2^+)/P^+$, and $\mathbf{k}_\perp = (1-\xi)\mathbf{p}_{1\perp} - \xi\mathbf{p}_{2\perp}$, $\mathbf{K}_\perp = (1-\eta)(\mathbf{p}_{1\perp} + \mathbf{p}_{2\perp}) - \eta\mathbf{p}_{3\perp}$. In computing a form factor, we take quark 3 to be the one struck by the photon. The value of $1-\eta$ is not changed ($q^+ = 0$), so only one relative momentum, $\mathbf{K}_\perp$ is changed: $\mathbf{K}'_\perp = \mathbf{K}_\perp - \eta\mathbf{q}_\perp$. The form of the momentum distribution wave function is taken from Schlumpf [22]:

$$\Phi(M_0) = N\left(M_0^2 + \beta^2\right)^\gamma, \tag{5}$$

with M_0^2 the mass-squared operator for a noninteracting system:

$$M_0^2 = \frac{K_\perp^2}{\eta(1-\eta)} + \frac{k_\perp^2 + M^2}{\eta\xi(1-\xi)} + \frac{M^2}{1-\eta}. \tag{6}$$

Schlumpf's parameters were $\beta = 0.607\,\mathrm{GeV}$, $\gamma = -3.5$, $M = 0.267\,\mathrm{GeV}$, where the value of γ was chosen so that $Q^4 G_M(Q^2)$ is approximately constant for $Q^2 > 4\,\mathrm{GeV}^2$, in accord with experimental data. The parameter β helps govern the values of the transverse momenta allowed by the wave function Φ and is closely related to the rms charge radius. The constituent quark mass, M, was primarily determined by the magnetic moment of the proton. We shall use different values when including the pion cloud and fitting lattice data.

A physical nucleon can sometimes undergo a quantum fluctuation so that it consists of a bare nucleon and a virtual pion. In this case, an incident photon can interact electromagnetically with a bare nucleon, Fig. 1(a), with a nucleon while a pion is present, Fig. 1(b), or with a charged pion in flight, Fig. 1(c). These effects are especially pronounced for the neutron G_E [6], at small values of Q^2. The tail of the negatively charged pion distribution extends far out into space, causing

the mean square charge radius, R_n^2, to be negative. The effects of the pion cloud need to be computed relativistically if one is to confront data taken at large Q^2. This involves evaluating the Feynman diagrams of Fig. 1 using photon-bare-nucleon form factors from the relativistic model, and using a relativistic π-nucleon form factor. The resulting model is defined as the light-front cloudy bag model LFCBM [19]. The light-front treatment is implemented by evaluating the integral over the virtual pion four-momentum $k^{\pm}$, $\mathbf{k}_\perp$, by first performing the integral over k^- analytically, reexpressing the remaining integrals in terms of relative variables ($\alpha = k^+/p^+$), and shifting the relative $_\perp$ variable to $\mathbf{L}_\perp$ to simplify the numerators. Thus the Feynman graphs, Fig. 1, are represented by a single τ-ordered diagram. The use of J^+ and the Yan identity [23] $S_F(p) = \sum_s u(p,s)\overline{u}(p,s)/(p^2 - m^2 + i\epsilon) + \gamma^+/2p^+$ allows one to see that the nucleon current operators appearing in Fig. 1(b) act between on-mass-shell spinors.

The results can be stated as

$$F_{i\alpha}(Q^2) = Z\big[F^{(0)}_{i\alpha}(Q^2) + F_{ib\alpha}(Q^2) + F_{ic\alpha}(Q^2)\big], \tag{7}$$

where $i = 1, 2$ denotes the Dirac and Pauli form factors, $\alpha = n, p$ determines the identity of the nucleon, and $F^{(0)}_{i\alpha}(Q^2)$ are the form factors computed in the absence of pionic effects. The wave function renormalization constant, Z, is determined from the condition that the charge of the proton be unity: $F_{1p}(Q^2 = 0) = 1$. For illustration we start with the calculation of the neutron form factors. Then, evaluating the graph in Fig. 1(b) gives

$$\begin{aligned} F_{1bn}(Q^2) = g_0^2 \int_0^1 d\alpha\alpha \int \frac{d^2L}{(2\pi)^3} R_N(\mathbf{L}^{(+)\,2}, \alpha) R_N(\mathbf{L}^{(-)\,2}, \alpha) \\ \times \big\{\big(F^{(0)}_{1p}(Q^2) + F^{(0)}_{1n}(Q^2)/2\big)[\alpha^2(M^2 - Q^2/4) + L^2] \\ - \big[F^{(0)}_{2p}(Q^2) + F^{(0)}_{2n}(Q^2)/2\big](\alpha^2 Q^2/2)\big\}, \end{aligned} \tag{8}$$

$$\begin{aligned} F_{2bn}(Q^2) = -g_0^2 \int_0^1 d\alpha\alpha \int \frac{d^2L}{(2\pi)^3} R_N(\mathbf{L}^{(+)\,2}, \alpha) R_N(\mathbf{L}^{(-)\,2}, \alpha) \\ \times \left\{\left(F^{(0)}_{1p}(Q^2) + \frac{1}{2}F^{(0)}_{1n}(Q^2)\right)(2\alpha^2 M^2) \right. \\ + \left(F^{(0)}_{2p}(Q^2) + \frac{1}{2}F^{(0)}_{2n}(Q^2)\right) \\ \left. \times \big[\alpha^2 M^2(1 - Q^2/4M^2) + \big(L_x^2 - L_y^2\big)\big]\right\} \end{aligned} \tag{9}$$

where g_0 is the bare πN coupling constant, and the renormalized coupling constant $Zg_0^2 = g^2/4\pi = 13.5$, $\mathbf{L}_\perp^{(\pm)} \equiv \mathbf{L}_\perp \pm \alpha\mathbf{q}_\perp/2$, $\alpha \equiv k^+/p^+$, $D_N(k_\perp^2, \alpha) \equiv M^2\alpha^2 + k_\perp^2 + \mu^2(1-\alpha)$, and $R_N(k_\perp^2, \alpha) \equiv [F^N_{\pi N}(k_\perp^2, \alpha)]/[D_N(k_\perp^2, \alpha)]$. The πN form factor is taken as [24,25]

$$F_{\pi N}(k_\perp^2, \alpha) = e^{-(D_N(k_\perp^2,\alpha)/2\alpha(1-\alpha)\Lambda^2)}, \tag{10}$$

and maintains charge conservation [27]. The constant Λ is a free parameter, but very large values are excluded by the small flavor asymmetry of the nucleon sea.

From Eqs. (8) and (9) we see that each term in the nucleon current operator contributes to both F_1 and F_2. The evaluation of graph 1(c) yields

$$\begin{aligned} F_{1cn}(Q^2) = -g_0^2 F_\pi(Q^2) \int_0^1 d\alpha\alpha \int \frac{d^2K}{(2\pi)^3} R(\mathbf{K}^{(+)\,2}, \alpha) \\ \times R(\mathbf{K}^{(-)\,2}, \alpha)\left[K^2 + M^2\alpha^2 - (1-\alpha)^2\frac{Q^2}{4}\right] \end{aligned} \tag{11}$$

$$\begin{aligned} F_{2cn}(Q^2) = -g_0^2(2M^2) F_\pi(Q^2) \int_0^1 d\alpha\alpha^2(1-\alpha) \\ \times \int \frac{d^2K}{(2\pi)^3} R(\mathbf{K}^{(+)\,2}, \alpha) R(\mathbf{K}^{(-)\,2}, \alpha), \end{aligned} \tag{12}$$

where $\mathbf{K}_\perp^{(\pm)} \equiv \mathbf{K}_\perp \pm (1-\alpha)\mathbf{q}_\perp/2$.[2]

The proton form factors can be obtained by simply making the replacements $n \to p$ in Eqs. (8), (9) and $-g_0^2 \to g_0^2$ in Eqs. (11), (12). The change in sign accounts for the feature that the π^- cloud of the neutron becomes a π^+ cloud for the proton. The mean-square isovector radii $\langle r^2\rangle_i^V$, computed using Eq. (7), and then taken to the chiral limit at low Q^2, have the same singular log terms as those of the relativistic results of Beg and Zepeda [26].

The LFCBM was defined by choosing four free parameters: $m, \beta, \gamma, \Lambda$ so as to best reproduce the four experimentally measured electromagnetic form factors of the nucleon [19]. In the present work, the most relevant of these parameters will be varied to reproduce lattice data, and the resulting dependence on the quark mass and lattice spacing used to extrapolate to the physical region.

III. FITTING THE QCDSF FORM FACTORS AND EXTRAPOLATING TO THE PHYSICAL PION MASS

In this section we discuss the fitting procedure used to parametrize the nucleon form factors calculated in lattice QCD. We use data produced by the QCDSF Collaboration [12] and employ the LFCBM to calculate the corresponding form factors, varying the model parameters to find the best fit to the different sets of lattice data obtained for different values of the current quark mass, m_q. The behavior of the fitting parameters is then represented by a polynomial function of the quark mass m_q. This polynomial fit in m_q, or equivalently in pion mass squared, m_π^2, can then be used to extrapolate the values of the fitting parameters to the physical pion mass. Nucleon form factors for the physical pion mass are then calculated using the extrapolated values for the model parameters. In the following few subsections a more elaborate explanation is given and the results are presented. In Sec. III A we describe the available data and the analysis procedure used to extract the quantities necessary for further fits. In Sec. III B we describe the details of the fitting and extrapolation process and in the Sec. III C we present the nucleon form factors resulting

[2]These formulas are slightly different from those of Ref. [19]. This leads to slight changes in the parameters that will be discussed elsewhere.

from the extrapolation to the physical pion mass and make comparisons with experiment.

A. QCDSF data and its analysis

The form factor calculations in Ref. [12] were carried out for three different values of the lattice spacing, $a = \{0.47, 0.34, 0.26\}\,\mathrm{GeV}^{-1}$. For each value of a several sets of pion (or equivalently nucleon) masses were considered. For each mass set Dirac and Pauli form factors for both the proton and neutron were calculated at several values of Q^2. The typical range for the pion mass used varied from 1.2 to 0.6 GeV, with the corresponding nucleon mass ranging from approximately 2 to 1.5 GeV. The typical range for Q^2 was 0.6 to 2.3 GeV^2.

The LFCBM is basically a relativistic constituent quark model, so we need to relate the model constituent mass of Eq. (6) to the masses of the nucleon and pion. To do so we use the approach of Ref. [18], [Eq. (8)]

$$M = M_\chi + \frac{c m_q^{\mathrm{phys}}}{\left(m_\pi^{\mathrm{phys}}\right)^2} m_\pi^2, \tag{13}$$

where M_χ is the constituent quark mass in the chiral limit, m_q^{phys} is the current quark mass and c is of order 1. In the study of octet magnetic moments in the AccessQM model of Ref. [18], the best fit value for M_χ was 0.42 GeV, while for $c m_q^{\mathrm{phys}}$ it was 0.0059 GeV.

B. Lattice data fit and extrapolation

The first step in our extrapolation of the lattice results to the physical quark mass is to fit the lattice results for each quark mass m_q by adjusting the parameters of the LFCBM calculation. For that purpose two fitting parameters were chosen. The first parameter is M_χ in Eq. (13), which determines the constituent quark mass. This parameter was varied for each lattice spacing separately, since some dependence upon lattice spacing was anticipated. The second parameter is the internal parameter, γ, in the nucleon wave function Eq. (5), which is varied separately for each pion (or equivalently nucleon) mass. For convenience, we express all magnetic form factors G_M in "physical" units of $e/2M_N^{\mathrm{Physical}}$. Since the LFCBM uses the mass of the ρ meson included in the pion electromagnetic form factor, we need the extrapolated value for its mass. We use the simple fitting function from Ref. [28]:

$$m_\rho = c_0 + c_1 m_\pi^2, \tag{14}$$

with $c_0 = 0.776\,\mathrm{GeV}$ and $c_1 = 0.427\,\mathrm{GeV}^{-1}$.

A function representing the χ^2 for the deviation between the lattice data and the values calculated using the LFCBM was constructed and minimized by varying the fitting parameters. Changing the value of M_χ causes the calculated form factors to move up or down by an amount approximately independent of Q^2, thereby causing a relatively small change in χ^2. Therefore a simple grid variation for that parameter was employed, with grid boundaries $M_\chi \in [0.15, 0.45]$ GeV, and step size of $\delta_{M_\chi} = 0.01$ GeV. As for the parameter, γ, the variation of χ^2 was much stronger and the Minuit package of CERN's

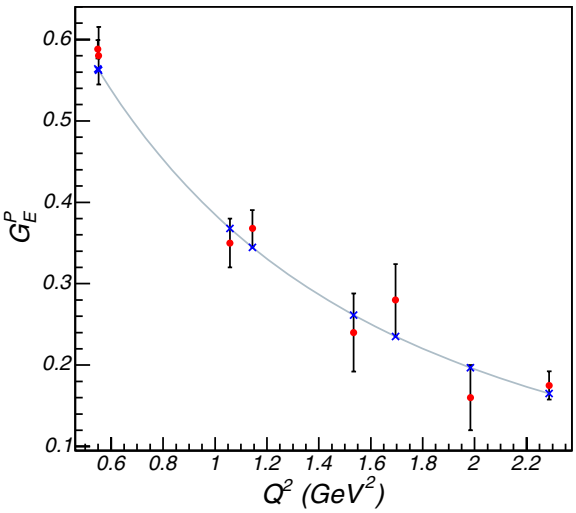

FIG. 2. (Color online) LFCBM fit to QCDSF data for G_E^P (in units of e) for a lattice spacing $a = 0.26\,\mathrm{GeV}^{-1}$, $M_P = 1.80$ GeV, and $m_\pi = 0.93$ GeV.

Root framework [29] was used for the minimization. At first the boundaries for γ were set to keep it in the physical region, but successful boundless runs were also performed in order to confirm the true minimum and error sizes. The pion masses used in the lattice calculation are very large, and the resulting pionic effects are very small. Therefore the value of Λ could not be determined from lattice data and its value was held fixed at $\Lambda = 0.58$ GeV Similarly, varying β did not change the description of the lattice data, so it was held fixed at $\beta = 0.607\,\mathrm{GeV}/c$. The resulting fits are in good agreement with data, as one can see in Figs. 2–5. The best-fit values of the parameters are shown in Table I. The figures show results for the smallest lattice spacing, $a = 0.26\,\mathrm{GeV}^{-1}$, but the reproduction of lattice data is equally successful for larger values of a.

The next step is to extrapolate the fitting parameters to the physical quark mass. This is done using the assumption that the parameters vary smoothly as functions of the quark mass, and the fact that $m_q \sim m_\pi^2$ over the mass range investigated. We limited the extrapolation function to a low order polynomial in m_π^2. The resulting fits for two lattice spacings are presented in Figs. 6 and 7, from which we see that the fitting function provides a very accurate representation of the values obtained from lattice data. The fitted values of γ and the extrapolation to the physical value of m_π, with their corresponding errors, are shown in Figs. 6 and 7.

In our calculations, M_χ has a very weak dependence on the pion mass, but it has a rather strong dependence upon the lattice spacing. As we see in Table I and Figs. 2–5, very good fits to the lattice data are obtained even without varying M_χ for each quark mass. By contrast, Fig. 8 and Table I show rather dramatic variation of M_χ for different values of the lattice spacing, a. This suggests that the larger values of the lattice spacing are rather far from the continuum limit and (at best) only the results for the smallest lattice spacing should be compared with experimental data. It would clearly be desirable

TABLE I. Lattice data and LFCBM fitting parameters. (All expressed in powers of GeV.)

a	m_π	M_N	M_χ	γ
0.47	1.146	2.062	0.390(5)	−6.12(7)
0.47	1.068	1.981	0.390(5)	−5.67(6)
0.47	0.873	1.746	0.390(5)	−4.95(9)
0.47	0.752	1.567	0.390(5)	−4.78(12)
0.47	0.638	1.503	0.390(5)	−4.67(15)
0.47	*0.135*	*0.938*	*0.390(5)*	*−4.79(46)*
0.34	1.201	2.141	0.280(5)	−5.03(6)
0.34	1.035	1.933	0.280(5)	−4.37(5)
0.34	0.881	1.732	0.280(5)	−4.99(5)
0.34	0.706	1.522	0.280(5)	−3.51(6)
0.34	*0.135*	*0.938*	*0.280(5)*	*−2.91(29)*
0.26	1.237	2.202	0.210(5)	−4.78(5)
0.26	1.092	2.028	0.210(5)	−4.14(7)
0.26	0.925	1.802	0.210(5)	−3.69(5)
0.26	0.744	1.600	0.210(5)	−3.09(6)
0.26	0.580	1.379	0.210(5)	−3.01(13)
0.26	*0.135*	*0.938*	*0.210(5)*	*−2.41(22)*

to have new data at even smaller a, or using an improved action, known to provide a good approximation to the continuum limit.

Use of the values of γ, M determined by the lattice data in the LFCBM defines a lattice version of the LFCBM. We may use this new model to compute the form factors at arbitrarily large values of Q^2, thereby extending the kinematic range of the lattice calculations. The results are shown in Figs. 9–12. In Figs. 13 and 14 we show the corresponding plots of $\mu_0 G_E/G_M$.

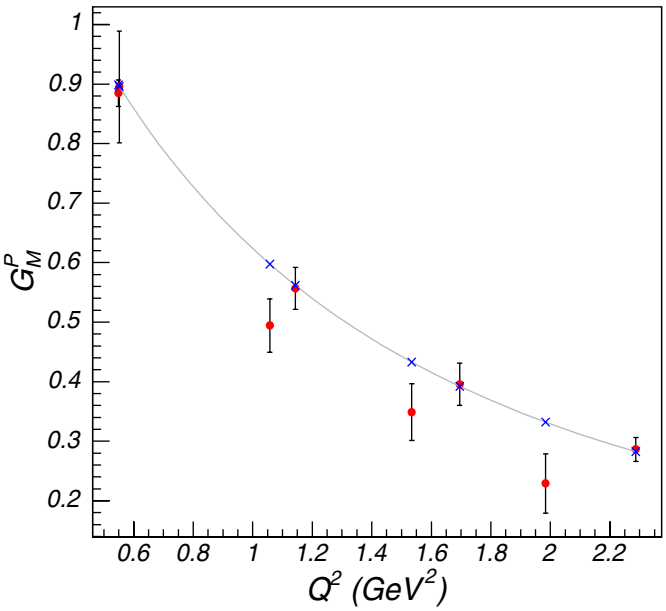

FIG. 3. (Color online) LFCBM fit to QCDSF data for G_M^P [in units of $e/(2M_N^{\text{Physical}})$] for a lattice spacing $a = 0.26\,\text{GeV}^{-1}$, $M_P = 1.80\,\text{GeV}$, and $m_\pi = 0.93\,\text{GeV}$.

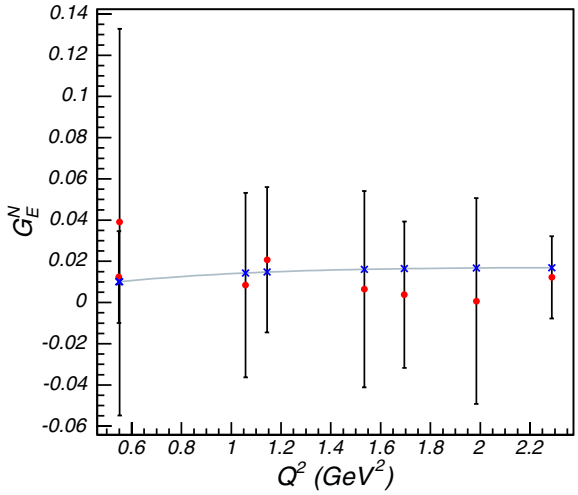

FIG. 4. (Color online) LFCBM fit to QCDSF data for G_E^N (in units of e) for a lattice spacing $a = 0.26\,\text{GeV}^{-1}$, $M_P = 1.80\,\text{GeV}$, and $m_\pi = 0.93\,\text{GeV}$.

C. Results at the physical pion mass and comparison with experiment

We use the extrapolated values of γ and M (Figs. 6–8) to calculate the nucleon electric and magnetic form factors using the physical pion and nucleon masses. The resulting plots for G_E, G_M and their ratios vs Q^2 for both proton and neutron are shown in Figs. 15–20. Figure 17 shows that our results are in more or less good agreement with the experimental data in the low-Q^2 region, but yield a slightly lower value of Q^2 for the zero crossover point than that extrapolated from experiment [30]. A new analysis that includes an estimate of all of the effects of two photon exchange yields a zero-crossing value that is somewhat closer to ours [31] but future data will resolve this unambiguously.

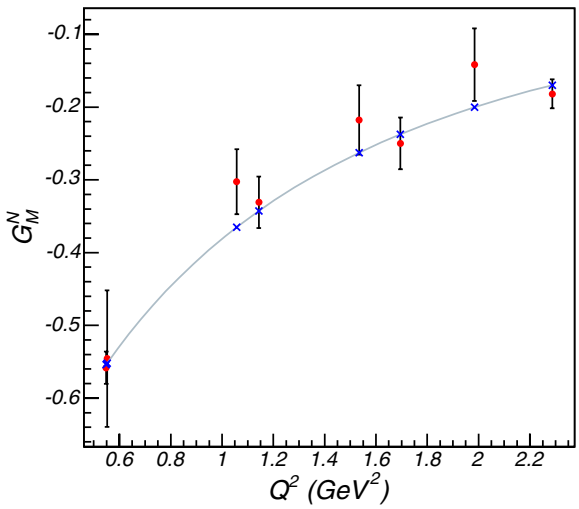

FIG. 5. (Color online) LFCBM fit to QCDSF data for G_M^N [in units of $e/(2M_N^{\text{Physical}})$] for a lattice spacing $a = 0.26\,\text{GeV}^{-1}$, $M_P = 1.80\,\text{GeV}$, and $m_\pi = 0.93\,\text{GeV}$.

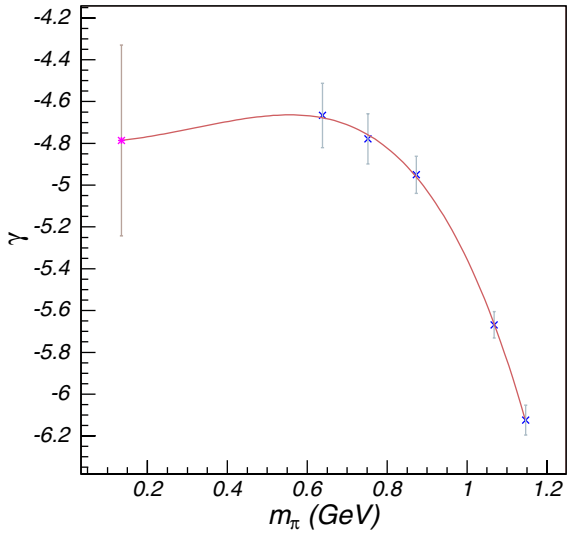

FIG. 6. (Color online) Polynomial extrapolation of γ vs m_π for lattice spacing $a = 0.47$ GeV^{-1}.

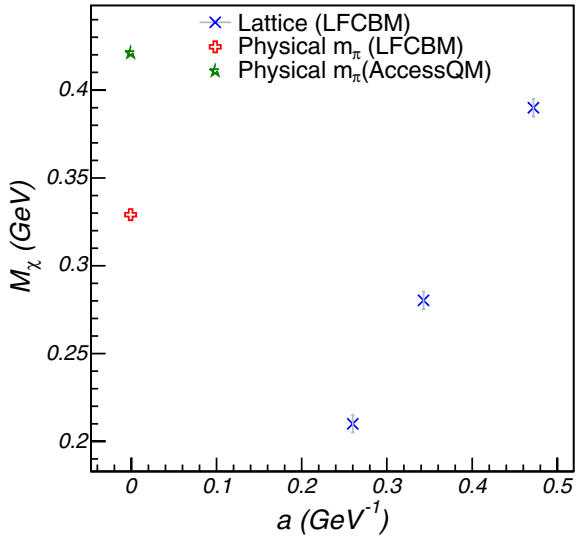

FIG. 8. (Color online) Variation of M_χ with lattice spacing a. The best-fit values of M_χ for physical m_π using LFCBM and AccessQM models are presented as well.

An alternative method of determining the value of the Q^2 for which G_E/G_M passes through zero at the physical pion mass is to fit the crossover values as a linear function of m_π^2 and extrapolate again to the physical pion mass. The resulting plot is shown in Fig. 21. This procedure yields approximately the same crossover point as found in Fig. 17.

IV. DISCUSSION

Our study of the form factors calculated using the LFCBM with parameters determined by lattice data and by extrapolation to the physical pion masses yields very interesting results. The ratio G_E^p/G_M^p passes through zero for all of the calculations. The main variation of the position of the crossover between the fitting curves shown in Figs. 13 and 14 comes from the variation of the nucleon mass, and not the variation of γ. Even though for the physical pion mass, the ratio varies rapidly as a function of γ in the region $\gamma \sim -2$, the function G_E/G_M for the neutron has a turning point at about $\gamma \sim -2.3$. We shall explain these features using the LFCBM.

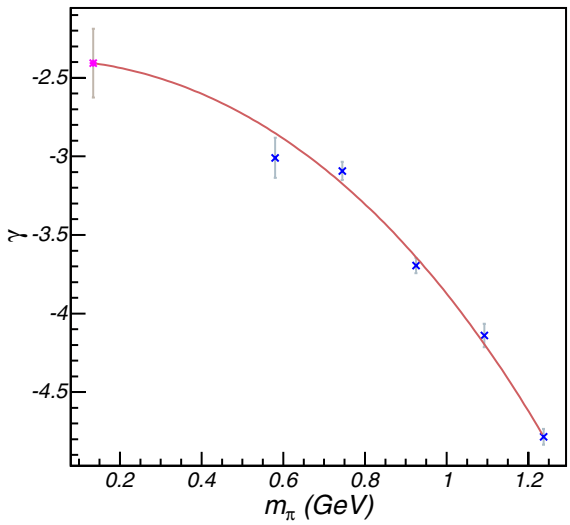

FIG. 7. (Color online) Polynomial extrapolation of γ vs m_π for lattice spacing $a = 0.26$ GeV^{-1}.

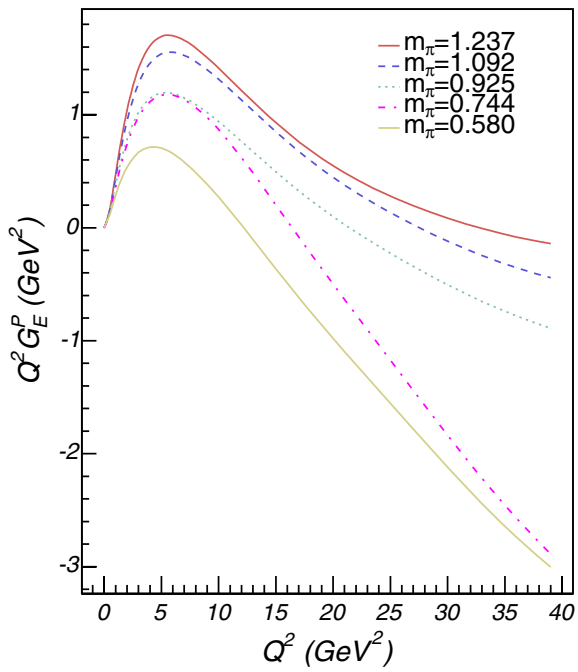

FIG. 9. (Color online) LFCBM calculations using parameters (Figs. 6–8) obtained by fitting the lattice results for the proton electric form factor, G_E, at lattice spacing $a = 0.26$ GeV^{-1}.

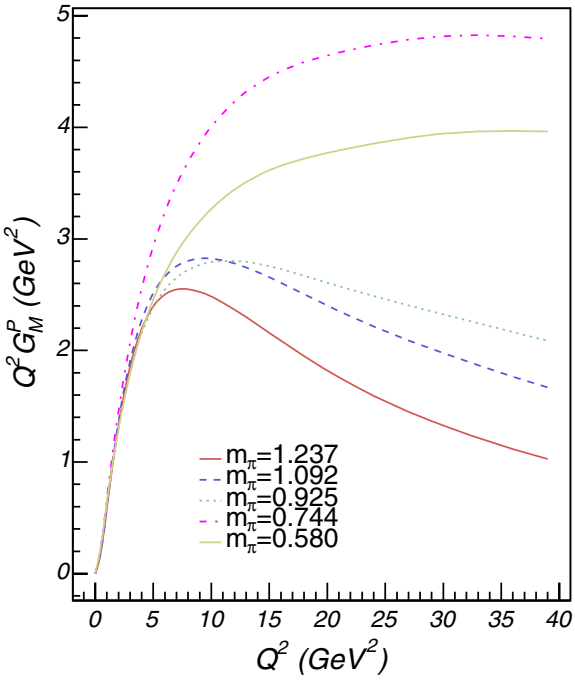

FIG. 10. (Color online) LFCBM calculations using parameters (Figs. 6–8) obtained by fitting the lattice results for the proton magnetic form factor, G_M, at lattice spacing $a = 0.26$ GeV^{-1}.

Let us express the ratio G_E/G_M in terms of Pauli and Dirac form factors, F_1 and F_2, respectively, using Eq. (3)

$$\frac{G_E}{G_M} = \frac{F_1 - Q^2/(4M_N^2)F_2}{F_1 + F_2} = 1 - \frac{1 + Q^2/(4M_N^2)}{1 + F_1/F_2}. \qquad (15)$$

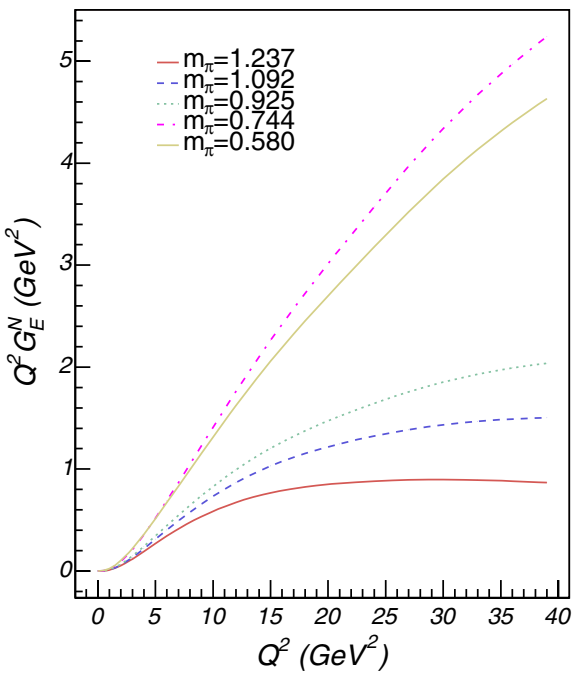

FIG. 11. (Color online) LFCBM calculations using parameters (Figs. 6–8) obtained by fitting the lattice results for the neutron electric form factor, G_E, at lattice spacing $a = 0.26$ GeV^{-1}.

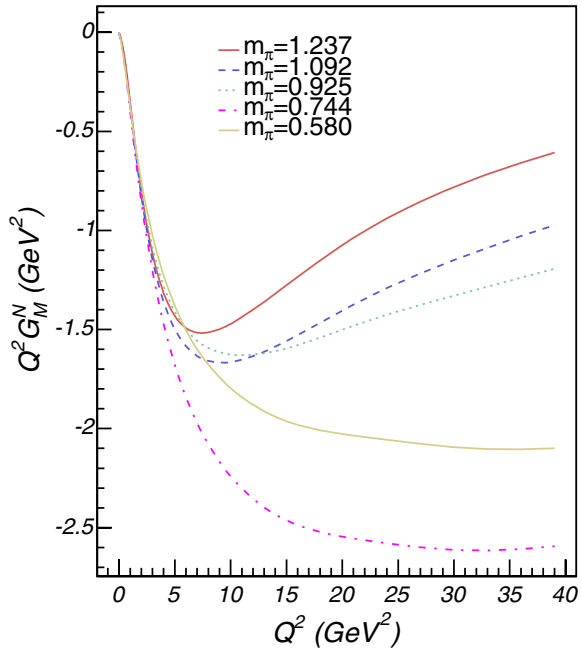

FIG. 12. (Color online) LFCBM calculations using parameters (Figs. 6–8) obtained by fitting the lattice results for the neutron magnetic form factor, G_M, at lattice spacing $a = 0.26$ GeV^{-1}.

Consider first the values of $Q^2 = (Q^2_{\text{Cross}})$ where the ratio G_E/G_M for the proton passes through zero for the set of calculations shown in Fig. 13. Equation (15) tells us that

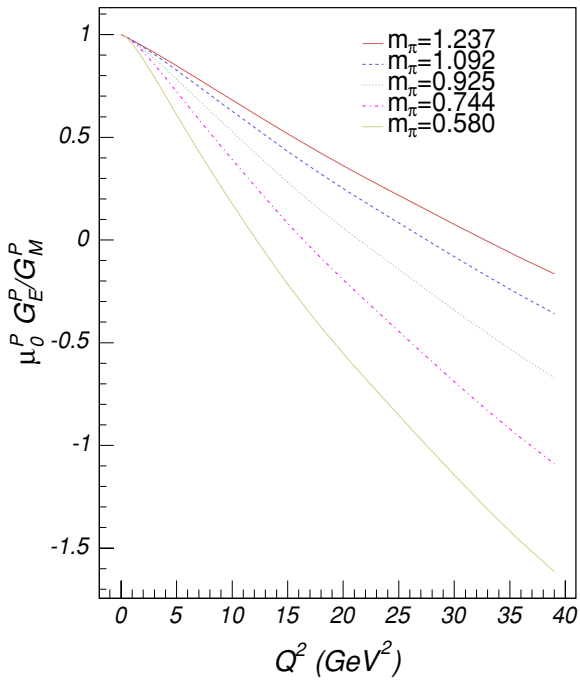

FIG. 13. (Color online) LFCBM calculations using parameters (Figs. 6–8) obtained by reproducing lattice results for the ratio of proton form factors, $\mu_0 G_E/G_M$, at lattice spacing $a = 0.26$ GeV^{-1}.

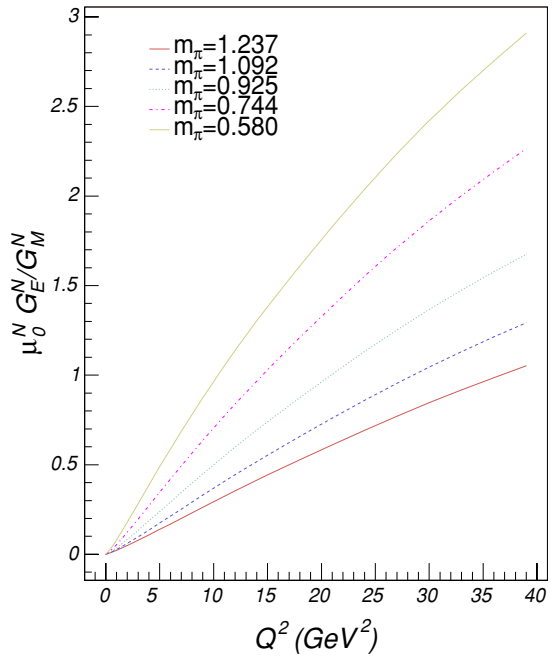

FIG. 14. (Color online) LFCBM calculations using parameters (Figs. 6–8) obtained by reproducing lattice results for the ratio of neutron form factors, $\mu_0 G_E/G_M$, at lattice spacing $a = 0.26$ GeV^{-1}.

$$Q^2_{\text{Cross}} = 4M_N^2 \frac{F_1}{F_2}. \tag{16}$$

Now let us consider the formula for $F_{i\alpha}(Q^2)$, Eq. (7). The second and third terms in Eq. (7) are only significant in the *low*-Q^2 region for physical pion masses. In the *high*-Q^2 region,

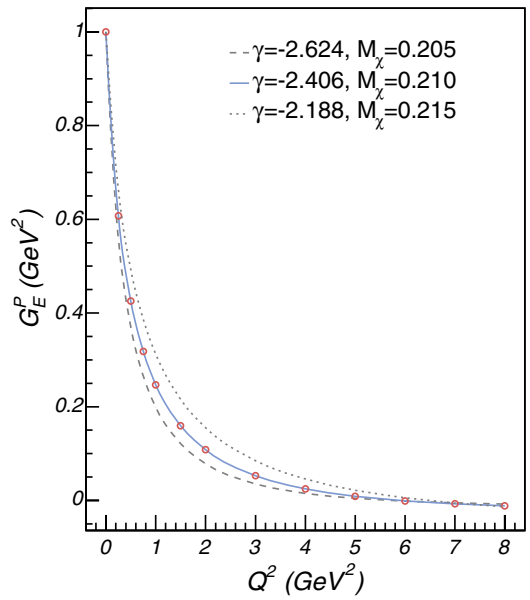

FIG. 15. (Color online) Extrapolated calculations for the proton electric form factor, G_E, for lattice spacing $a = 0.26$ GeV^{-1}. The dashed and dotted curves show the upper and lower limits of variation of the calculated values due to the uncertainties of the parameters γ and M_χ.

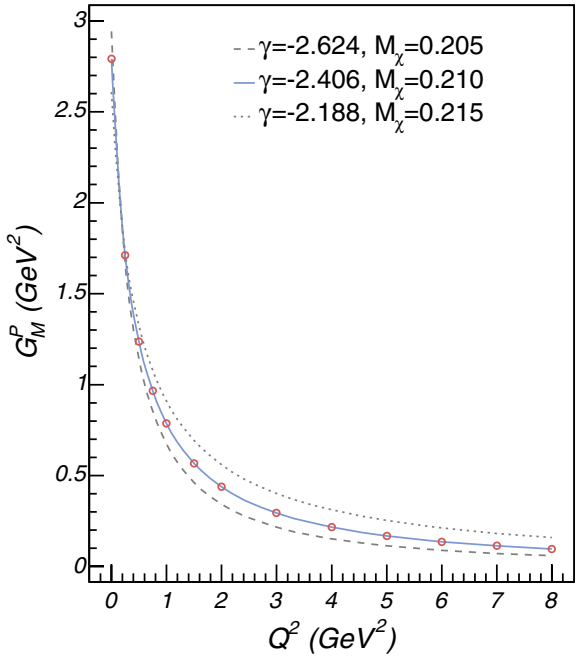

FIG. 16. (Color online) Extrapolated calculations for the proton magnetic form factor, G_M, for lattice spacing $a = 0.26$ GeV^{-1}. The dashed and dotted curves show the upper and lower limits of variation of the calculated values due to the uncertainties of the parameters γ and M_χ.

or for lattice calculations with high pion mass, these terms are vanishingly small. Indeed the numerical calculations support

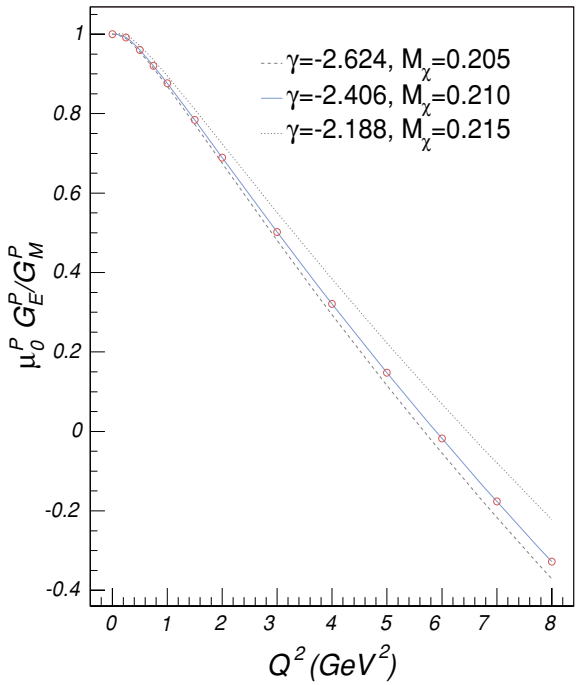

FIG. 17. (Color online) Extrapolated calculations for the ratio of proton form factors, $\mu_0 G_E/G_M$, for lattice spacing $a = 0.26$ GeV^{-1}. The dashed and dotted curves show the upper and lower limits of variation of the calculated values due to the uncertainties of the parameters γ and M_χ.

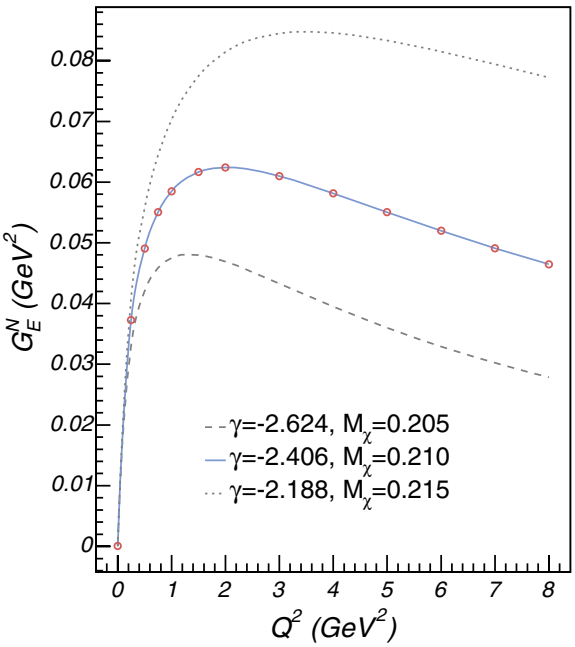

FIG. 18. (Color online) Extrapolated calculations for the neutron electric form factor, G_E, for lattice spacing $a = 0.26$ GeV^{-1}. The dashed and dotted curves show the upper and lower limits of variation of the calculated values due to the uncertainties of the parameters γ and M_χ.

these statements, so we can neglect their contribution in the rest of the discussion.

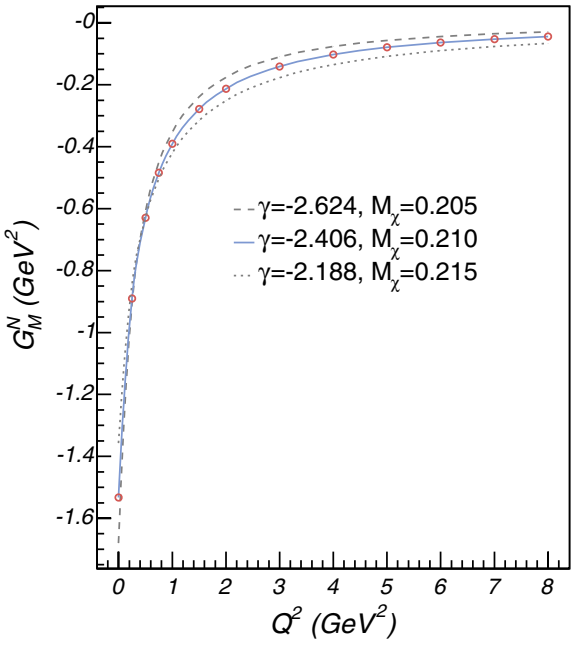

FIG. 19. (Color online) Extrapolated calculations for the neutron magnetic form factor,G_M, for lattice spacing $a = 0.26$ GeV^{-1}. The dashed and dotted curves show the upper and lower limits of variation of the calculated values due to the uncertainties of the parameters γ and M_χ.

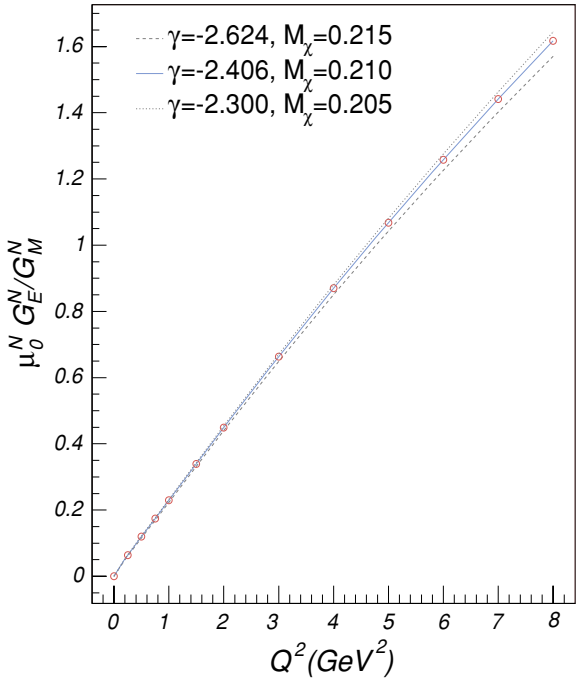

FIG. 20. (Color online) Extrapolated calculations for the ratio of neutron form factors, $\mu_0 G_E/G_M$, for lattice spacing $a = 0.26$ GeV^{-1}. The dashed and dotted curves show the upper and lower limits of variation of the calculated values due to the uncertainties of the parameters γ and M_χ.

The corresponding formulas for $F_1^{(0)}$ and $F_2^{(0)}$ from Ref. [20] are

$$F_1^{(0)}(Q^2) = \int \frac{d^2q_\perp d\xi}{\xi(1-\xi)} \frac{d^2K_\perp d\eta}{\eta(1-\eta)} \tilde{\Phi}^\dagger(M_0')\tilde{\Phi}(M_0) \times \left\langle \chi_0^{\rm rel}(\mathbf{p}_1', \mathbf{p}_2')|\chi_0^{\rm rel}(\mathbf{p}_1, \mathbf{p}_2)\right\rangle \langle \uparrow \mathbf{p}_3'|\uparrow \mathbf{p}_3\rangle \quad (17)$$

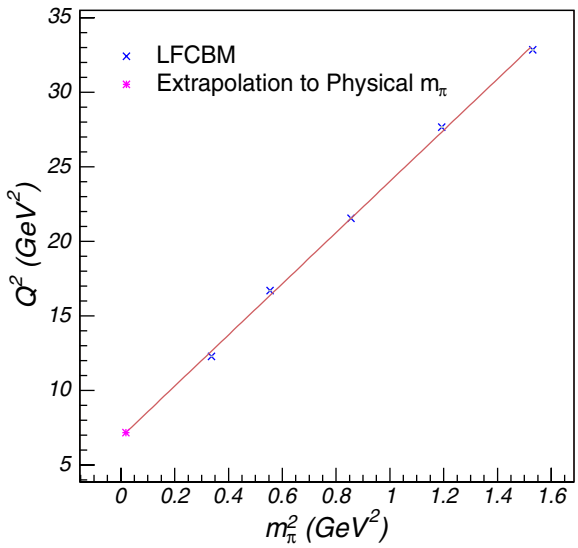

FIG. 21. (Color online) Extrapolation of $Q^2_{\rm Cross}$ where G_E/G_M passes through zero for lattice spacing $a = 0.26$ GeV^{-1}.

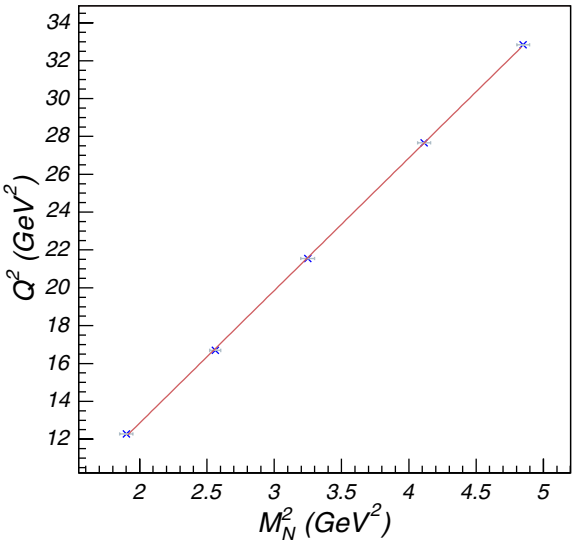

FIG. 22. (Color online) Linear fit of $Q^2_{\rm Cross}$ where G_E/G_M passes through zero for lattice spacing $a = 0.26$ GeV^{-1}.

$$\frac{QF_2^{(0)}(Q^2)}{2M_N} = \int \frac{d^2q_\perp d\xi}{\xi(1-\xi)} \frac{d^2K_\perp d\eta}{\eta(1-\eta)} \tilde{\Phi}^\dagger(M_0')\tilde{\Phi}(M_0) \times \langle \chi_0^{\rm rel}(\mathbf{p}_1', \mathbf{p}_2')|\chi_0^{\rm rel}(\mathbf{p}_1, \mathbf{p}_2)\rangle \langle \uparrow \mathbf{p}_3'|\downarrow \mathbf{p}_3\rangle. \tag{18}$$

The $\tilde{\Phi}(M_0)$ factors are wave functions of the form of Eq. (5), but using the lattice values of γ, M shown in Figs. 6–8. We stress that these two integrals differ only by the last factor, which gives the spin nonflip and spin-flip dependence of $F_1^{(0)}$ and $QF_2^{(0)}/2M_N$, respectively. At high Q^2 these matrix elements are each of order Q, causing the ratio QF_2/F_1 to be approximately constant. So we can express $Q^2_{\rm Cross}$ as

$$Q^2_{\rm Cross} = 4M_N^2 \left(\frac{\int_{\uparrow\uparrow}}{\int_{\uparrow\downarrow}}\right)^2, \tag{19}$$

where $\int_{\uparrow\uparrow}$ denotes the integral for $F_1^{(0)}$, and $\int_{\uparrow\downarrow}$ denotes the integral for $F_2^{(0)}$.

In the high-Q^2 region the ratio in Eq. (19) is approximately a constant, because the difference comes only from the overlap factors of the spin-dependent parts of the wave functions in the integrals (see [9,19]). So the behavior of $Q^2_{\rm Cross}$ is governed primarily by the factor M_N^2. The linear variation of $Q^2_{\rm Cross}$ vs M_N^2 presented in Fig. 22 shows the validity of this interpretation.

We can also understand the behavior of G_E/G_M versus γ, by considering its role in the wave function. The factor γ determines the size of the momenta appearing in the integrands of Eqs. (17) and (18). The corresponding integrands differ by terms that are ratios of second order polynomials of the integration variables. For large absolute values of γ, the high momenta are cut off more strongly, so that the contribution of terms that cause differences between the integrals are not very significant. For small absolute values of γ the integrals become more sensitive to those terms and we obtain a larger variation of the ratios of the integrals and hence the ratio G_E/G_M.

V. CONCLUSION

We have seen that the LFCBM can produce a very good description of the lattice QCD data for the nucleon form factors over a wide range of quark masses with a smooth, analytic variation of the wave function parameter, γ, and the constituent quark mass, M. The pion cloud plays very little role in the mass range for which the lattice simulations have been made but it rapidly becomes more important as we approach the chiral limit. From the rather strong dependence of the form factors on the lattice spacing, a, it is not yet clear that we have obtained a good approximation to the continuum limit, but the form factors obtained at the smallest value of a are in reasonable agreement with experimental data in the low-Q^2 region for which the lattice simulations were made.

At present the lattice simulations are limited to values of the momentum transfer at or below $2\,\text{GeV}^2$ and it is therefore a very big extrapolation to look at the behavior of the form factors in the region of greatest current interest. Nevertheless, the behavior of G_E/G_M which we find is particularly interesting. The ratio crosses zero for all values of the quark mass but the position where this happens varies over a very wide range of Q^2. This variation can be understood almost entirely in terms of the variation of the corresponding nucleon mass, given that the ratio QF_1/F_2 is approximately Q^2 independent in the model. We obtain the same value of Q^2 for the crossover whether we extrapolate the position as a function of quark mass or simply evaluate the form factors at the physical pion mass, using the fitted dependence of the wave function parameters on pion mass.

In the immediate future it is clearly very important to improve on the lattice data, both by ensuring that we really have a good approximation to the continuum limit (e.g., by using a suitably improved action) and by extending the calculations to higher values of Q^2. It would also be important to remove the need for quenching, even though that may not be such a limitation at large Q^2. From the point of view of developing a deeper understanding of QCD itself it is important that the LFCBM is able to describe the present lattice data over such a wide range of masses. We would encourage a similar exercise for other models as a novel test of their validity. It remains to be seen whether the LFCBM has indeed been successful in predicting the behavior of the form factors at higher Q^2 and indeed whether it will match future experimental data.

ACKNOWLEDGMENTS

This work was supported in part by the U.S. National Science Foundation (Grant No. 0140300), the Southeastern Universities Research Association (SURA), U.S. DOE Grant No. DE-AC05-84ER40150, under which SURA operates Jefferson Lab, and also DOE Grant No. DE-FG02-97ER41014. G.A.M. thanks Jefferson Lab for its hospitality during the course of this work. H.H.M. thanks the Graduate School of Louisiana State University for partially supporting his research.

[1] A. W. Thomas and W. Weise, *The Structure of the Nucleon* (Wiley-VCH, New York, 2001).
[2] T. Reichelt *et al*. (Jefferson Laboratory E93-038 Collaboration), Eur. Phys. J. A **18**, 181 (2003).
[3] D. I. Glazier *et al*., nucl-ex/0410026.
[4] J. Friedrich and T. Walcher, Eur. Phys. J. A **17**, 607 (2003).
[5] A. W. Thomas, Adv. Nucl. Phys. **13**, 1 (1984); G. A. Miller, Int. Rev. Nucl. Phys. **2**, 190 (1984).
[6] S. Théberge, A. W. Thomas, and G. A. Miller, Phys. Rev. D **22**, 2838 (1980); D **23**, 2106 (1981); A. W. Thomas, S. Théberge, and G. A. Miller, *ibid*. **24**, 216 (1981); S. Théberge, G. A. Miller, and A. W. Thomas, Can. J. Phys. **60**, 59 (1982); G. A. Miller, A. W. Thomas, and S. Théberge, Phys. Lett. **B91**, 192 (1980).
[7] M. K. Jones *et al.* (Jefferson Lab Hall A Collaboration), Phys. Rev. Lett. **84**, 1398 (2000).
[8] O. Gayou *et al*. (Jefferson Lab Hall A Collaboration), Phys. Rev. Lett. **88**, 092301 (2002).
[9] G. A. Miller, Phys. Rev. C **68**, 022201(R) (2003).
[10] M. R. Frank, B. K. Jennings, and G. A. Miller, Phys. Rev. C **54**, 920 (1996).
[11] P. L. Chung and F. Coester, Phys. Rev. D **44**, 229 (1991); F. Cardarelli and S. Simula, Phys. Rev. C **62**, 065201 (2000); R. F. Wagenbrunn, S. Boffi, W. Klink, W. Plessas, and M. Radici, Phys. Lett. **B511**, 33 (2001).
[12] M. Gockeler *et al.* (QCDSF Collaboration), Phys. Rev. D **71**, 034508 (2005).
[13] D. B. Leinweber, D. H. Lu, and A. W. Thomas, Phys. Rev. D **60**, 034014 (1999).
[14] E. J. Hackett-Jones, D. B. Leinweber, and A. W. Thomas, Phys. Lett. **B489**, 143 (2000).
[15] T. R. Hemmert and W. Weise, Eur. Phys. J. A **15**, 487 (2002).
[16] R. D. Young, D. B. Leinweber, and A. W. Thomas, Phys. Rev. D **71**, 014001 (2005).
[17] J. D. Ashley *et al*., Eur. Phys. J. A **19**, 9 (2004); A. W. Thomas *et al*., Nucl. Phys. **A721**, 915 (2003).
[18] I. C. Cloet, D. B. Leinweber, and A. W. Thomas, Phys. Rev. C **65**, 062201(R) (2002).
[19] G. A. Miller, Phys. Rev. C **66**, 032201(R) (2002).
[20] G. A. Miller and M. R. Frank, Phys. Rev. C **65**, 065205 (2002).
[21] S. J. Brodsky and S. D. Drell, Phys. Rev. D **22**, 2236 (1980).
[22] F. Schlumpf, hep-ph/9211255.
[23] S. J. Chang and T. M. Yan, Phys. Rev. D **7**, 1147 (1973).
[24] V. R. Zoller, Z. Phys. C **53**, 443 (1992).
[25] H. Holtmann, A. Szczurek, and J. Speth, Nucl. Phys. **A596**, 631 (1996).
[26] M. A. B. Beg and A. Zepeda, Phys. Rev. D **6**, 2912 (1972).
[27] J. Speth and A. W. Thomas, Adv. Nucl. Phys. **24**, 83 (1997).
[28] D. B. Leinweber, A. W. Thomas, K. Tsushima, S. V. Wright, Phys. Rev. D **64**, 094502 (2001).
[29] http://root.cern.ch
[30] P. G. Blunden, W. Melnitchouk, and J. A. Tjon, Phys. Rev. Lett. **91**, 142304 (2003); Y. C. Chen, A. Afanasev, S. J. Brodsky, C. E. Carlson, M. Vanderhaeghen, *ibid*. **93**, 122301 (2004).
[31] J. Arrington, Phys. Rev. C **68**, 034325 (2003).